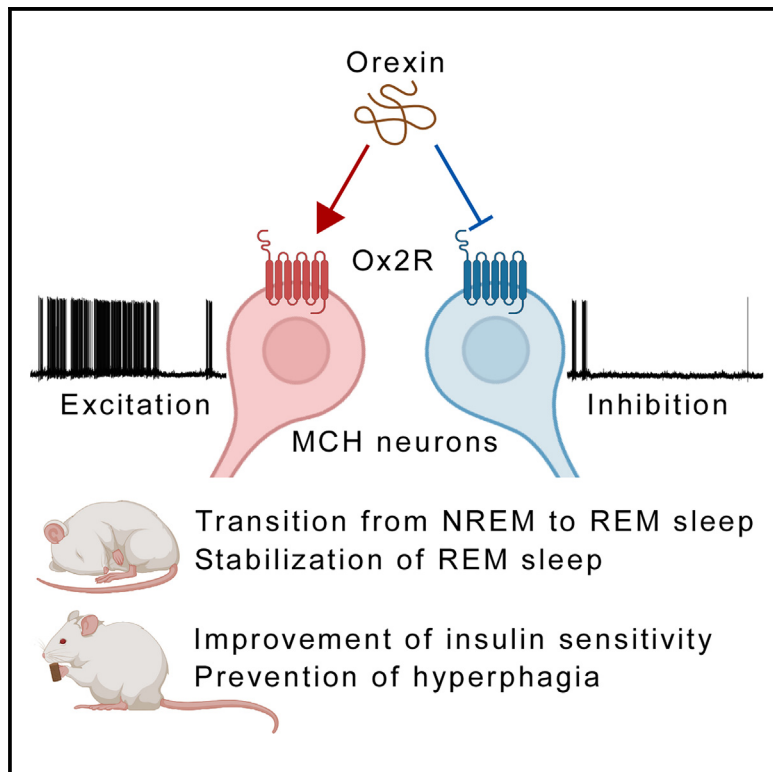


## Orexin/hypocretin receptor 2 signaling in MCH neurons regulates REM sleep and insulin sensitivity

### Graphical abstract



### Authors

Shuntaro Izawa, Debora Fusca,  
Hong Jiang, ..., Lukas Steuernagel,  
Peter Kloppenburg, Jens C. Brüning

### Correspondence

bruening@sf.mpg.de

### In brief

Izawa et al. show that orexin B induces both excitatory and inhibitory responses in distinct MCH neuron sub-populations. MCH-neuron-restricted Ox2R inactivation in female mice induces impairment of REM sleep and insulin sensitivity, indicating that Ox2R in MCH neurons regulates both sleep and metabolism.

### Highlights

- Ox2R is expressed in distinct molecular sub-populations of MCH neurons
- Orexin B elicits excitatory and inhibitory responses in MCH neurons
- Ox2R inactivation in MCH neurons impairs REM sleep in female mice
- Ox2R inactivation in MCH neurons impairs insulin sensitivity in female mice



## Report

# Orexin/hypocretin receptor 2 signaling in MCH neurons regulates REM sleep and insulin sensitivity

Shuntaro Izawa,<sup>1,2,3</sup> Debora Fusca,<sup>2,4</sup> Hong Jiang,<sup>1,2,3,5</sup> Christian Heilinger,<sup>1,2,3</sup> A. Christine Hausen,<sup>1,2,3</sup> F. Thomas Wunderlich,<sup>1,2,3</sup> Lukas Steuernagel,<sup>1,2,3</sup> Peter Kloppenburg,<sup>2,4</sup> and Jens C. Brüning<sup>1,2,3,6,7,\*</sup>

<sup>1</sup>Department of Neuronal Control of Metabolism, Max Planck Institute for Metabolism Research, Cologne, Germany

<sup>2</sup>Excellence Cluster on Cellular Stress Responses in Aging Associated Diseases (CECAD) and Center for Molecular Medicine Cologne (CMMC), University of Cologne, Cologne, Germany

<sup>3</sup>Policlinic for Endocrinology, Diabetes, and Preventive Medicine (PEDP), University Hospital Cologne, Kerpener Str. 62, 50937 Cologne, Germany

<sup>4</sup>Institute of Zoology, Department of Biology, University of Cologne, Cologne, Germany

<sup>5</sup>Department of Neurobiology, School of Basic Medical Sciences, Neuroscience Research Institute, Peking University, No. 38, Xueyuan Rd., Haidian District, Beijing 100191, China

<sup>6</sup>National Center for Diabetes Research (DZD), Neuherberg, Germany

<sup>7</sup>Lead contact

\*Correspondence: [bruening@sf.mpg.de](mailto:bruening@sf.mpg.de)

<https://doi.org/10.1016/j.celrep.2025.115277>

## SUMMARY

Orexin/hypocretin receptor type 2 (Ox2R), which is widely expressed in the brain, receives orexin signals and modulates sleep and metabolism. Ox2R selective agonists are currently under clinical trials for narcolepsy treatment. Here, we focused on Ox2R expression and function in melanin-concentrating hormone (MCH) neurons, which have opposite roles to orexin neurons in sleep and metabolism regulation. Ox2R-expressing MCH neurons showed heterogeneity of RNA expression, and orexin B application in brain slices induced both excitatory and inhibitory responses in distinct MCH neuron populations. Ox2R inactivation in MCH neurons reduced transitions from non-rapid eye movement (NREM) to REM sleep and impaired insulin sensitivity with excessive feeding after a fasting period in female mice. In conclusion, Ox2R mediates excitatory and inhibitory responses in MCH neuron sub-populations *in vivo*, which regulate sleep and metabolism in female mice.

## INTRODUCTION

The orexin/hypocretin system in the brain regulates both sleep and metabolism. Orexin maintains arousal and improves energy expenditure,<sup>1,2</sup> and deficiency of the orexin system results in narcolepsy, which is associated with irresistible sleep attacks and body weight gain.<sup>3</sup> Orexin peptides consist of two isopeptides, orexin A and orexin B.<sup>4</sup> Moreover, two orexin receptor subtypes have been identified as G-protein-coupled receptors (GPCRs): the orexin receptor type 1 (Ox1R), which exhibits an ~100-fold higher affinity for orexin A than for orexin B, whereas the Ox2R is a nonselective receptor for both orexin A and B.<sup>2</sup> Ox2R agonists for the treatment of narcolepsy are currently in development and undergoing clinical trials by several pharmaceutical companies.<sup>5–9</sup> However, the functional mechanisms of Ox2R action have not been fully defined. It is currently inconclusive whether Ox2R can exert an inhibitory effect via Gi proteins in addition to an excitatory effect via Gq proteins. Several *in vitro* studies with Ox2R-expressing cells have reported both Gq- and Gi-mediated responses, whereas the Gi response is weaker than the Gq response.<sup>10,11</sup> On the other hand, *ex vivo* studies employing patch-clamp recordings in

acute brain slices have so far reported only excitatory responses for orexin B or Ox2R agonists in any brain region or cell type investigated.<sup>12–15</sup> Thus, the endogenous inhibitory roles of Ox2R have not yet been established *in vivo*. Accordingly, the development of Ox2R agonists has largely focused on the Gq-mediated excitatory effect.<sup>5,16</sup>

Orexin-producing neurons and melanin-concentrating hormone (MCH)-producing neurons are located in the lateral hypothalamus, play opposing roles in several brain functions, and, remarkably, do not overlap in the expression of these critical neuropeptides as assessed by immunohistochemical staining.<sup>17</sup> In contrast to orexin neurons, MCH neurons accelerate sleep stages by inducing transitions from non-rapid eye movement sleep (NREMS) to REMS<sup>18</sup> and reduce energy expenditure and insulin sensitivity.<sup>19–21</sup> To maintain the functional balance in sleep and metabolism, orexin neurons inhibit MCH neurons via GABAergic interneurons, and glucose directly inhibits orexin neurons while directly exciting MCH neurons, indicating complex interdependent regulatory mechanisms.<sup>22–27</sup> In the present study, we investigated the potential direct regulatory role of orexin neurons on MCH neurons. We detected Ox2R expression in a subset of MCH neurons and hypothesized that Ox2R might



contribute to the orexin-neuron-mediated regulation of the MCH neuron circuitry. We revealed that the MCH neurons form distinct sub-populations and found not only excitatory but also inhibitory responses during orexin B application in perforated patch-clamp recordings in acute brain slices. Decreased expression of Ox2R in MCH neurons reduced transitions from NREMS to REMS, impaired insulin sensitivity, and caused hyperphagia in female mice. The sleep phenotype suggests an excitatory function of Ox2R in sleep-regulating MCH neurons, while the metabolic phenotype suggests an inhibitory function of Ox2R in metabolism-regulating MCH neurons. Therefore, Ox2R might exert excitatory and inhibitory functions in distinct sub-populations of MCH neurons that modulate sleep and metabolism in a sex-dependent manner.

## RESULTS

### Ox2Rs are expressed in molecularly distinct sub-populations of MCH neurons

To evaluate the expression pattern of orexin receptors in MCH neurons, we performed *in situ* hybridization of *Pmch* (MCH), *Hcrt1* (Ox1R), and *Hcrt2* (Ox2R) mRNA in the hypothalamus. Ox2R was expressed in over half of the MCH neurons, and this pattern was similar in male and female mice (Figures 1A and 1B). However, Ox1R showed a partially distinct expression pattern from Ox2R, and thus Ox2R(+) MCH neurons were classified into Ox1R(−)/Ox2R(+) and Ox1R(+)/Ox2R(+) MCH neurons, indicating molecularly distinct sub-populations of Ox2R(+) MCH neurons (Figures 1A and 1B).

Then, we performed single-nucleus (sn) RNA sequence experiments from 7,590 fluorescence-activated cell-sorted nuclei of MCH neurons isolated from *MCH-Cre; Isl-ZsGreen* mice, where MCH-neuron-restricted Cre expression allowed for the expression of ZsGreen in nuclei of MCH neurons. MCH neurons were classified into 10 clusters based on their RNA expression profiles (Figure 1C; Table S1A), where *Cartpt* and *Tacr3* expression delineated specific clusters of MCH neurons as previously identified<sup>28–33</sup> (Figures S1A and S1B). All 10 clusters exhibited expression of *Slc17a6*, while *Slc32a1* expression was largely absent, indicating that the vast majority of MCH neurons are glutamatergic, as has been demonstrated in recent studies<sup>29,30,34–36</sup> (Figures S1C and S1D). Ox2R expression was observed in 194 MCH neurons, mostly in the clusters 1, 2, 9, and 10, which were partially distinct from those characterized by Ox1R expression (Figures 1D and S2). The lower proportion of Ox1R- and Ox2R-expressing neurons in this experiment is consistent with a lower sensitivity of sn sequencing compared to the more sensitive RNA detection of the *in situ* hybridization experiments. This is similar to what we have previously observed also for Ox2R expression in the raphe nucleus.<sup>15</sup> Ox2R(+) MCH neurons in clusters 1, 2, 9, and 10 showed significantly different global RNA expression patterns between these clusters, indicating that Ox2R(+) MCH neurons are classified into molecularly distinct sub-populations (Figures 1E and 1F; Table S1B).

Since the coupling of both Gq and Gi with OxR2 has been described *in vitro*,<sup>10,11</sup> we analyzed the expression of components of these signaling cascades in Ox2R(+) MCH neurons. Interestingly, we found significant differences in the mRNA

expression levels of several genes related to Gi and Gq/s signaling<sup>37,38</sup> among distinct Ox2R(+) MCH neuron sub-populations (Figures 1G and 1H; Tables S1C and S1D). While we find components of both Gi and Gq signaling expressed in all clusters, there are clear differences in the expression levels of specific genes, especially between clusters 1 and 9/10 (Figure 1H). This includes, for example, higher expression levels of Gi-signaling components, such as *Adcy5* and *Rgs11*, and lower levels of Gq-signaling related components, like *Plcb1* and *Adcy2*, in cluster 1 compared to 9 and 10.<sup>38</sup> However, expression of the critical mediator of Gi-signaling *Kir3*<sup>37</sup> encoded by the *Kcnj3* is also overrepresented in clusters 9 and 10. Collectively, these data indicate that different OxR2-expressing MCH neuron clusters may exert a differential propensity for Gq/s vs. Gi coupling, while the functional consequences of these differences in gene expression remain unclear at this point.

### Orexin B evokes both excitatory and inhibitory responses in distinct populations of MCH neurons

Based on these observations and to investigate the responses mediated via Ox2R in individual MCH neurons, we performed electrophysiological recordings in acute brain slices from 24 tdTomato-labeled MCH neurons in *MCH-Cre; Isl-tdTomato* mice, where Cre-dependent excision of a loxP-flanked transcriptional STOP cassette allows for tdTomato expression specifically in MCH neurons (Figures 2A and 2C). The recordings were performed in a perforated patch-clamp configuration to conserve the integrity of the cytosolic pathways, and the MCH neurons were pharmacologically isolated from ionotropic synaptic inputs to minimize indirect modulatory effects. 100 nM orexin B was bath applied for 10 min. By comparing the action potential frequency of 5 min intervals directly before and at the end of the orexin B application (see STAR Methods), we classified 16 neurons (~67%) as orexin B inhibited and 5 neurons (~20%) as nonresponsive to orexin B. Moreover, we categorized 3 neurons (~13%) as orexin B excited (Figures 2B and 2D). In 2 of these neurons, orexin B dramatically increased the action potential frequency for ~2 min before the neurons stopped firing. This is consistent with the previously observed high rates of spike frequency adaptation or even spike failure during action potential bursts induced by the pronounced depolarization.<sup>39</sup> Taken together, these data indicate that orexin B, presumably via Ox2R modulation, inhibits a subset of MCH neurons and excites another subset of MCH neurons.

### Ox2R inactivation in MCH neurons impairs REMS

To functionally characterize the role of Ox2R-dependent signaling in MCH neurons, we crossed mice expressing the Cre recombinase under the control of the MCH promotor (*MCH-Cre*) with those allowing for Cre-dependent inactivation of the loxP-flanked exon 2 of the Ox2R gene (*Ox2R f/f*), resulting in *Ox2RΔMCH* (*MCH-Cre; Ox2R f/f*) mice, while *Ox2R f/f* littermates served as controls. To assess the efficiency and specificity of Ox2R inactivation in *Ox2RΔMCH* mice, we performed a BASE scope-based analysis of the mRNA expression encoded by exon 2 of the Ox2R (*Hcrt2*) gene in the different groups of mice. This analysis revealed that exon 2 mRNA expression

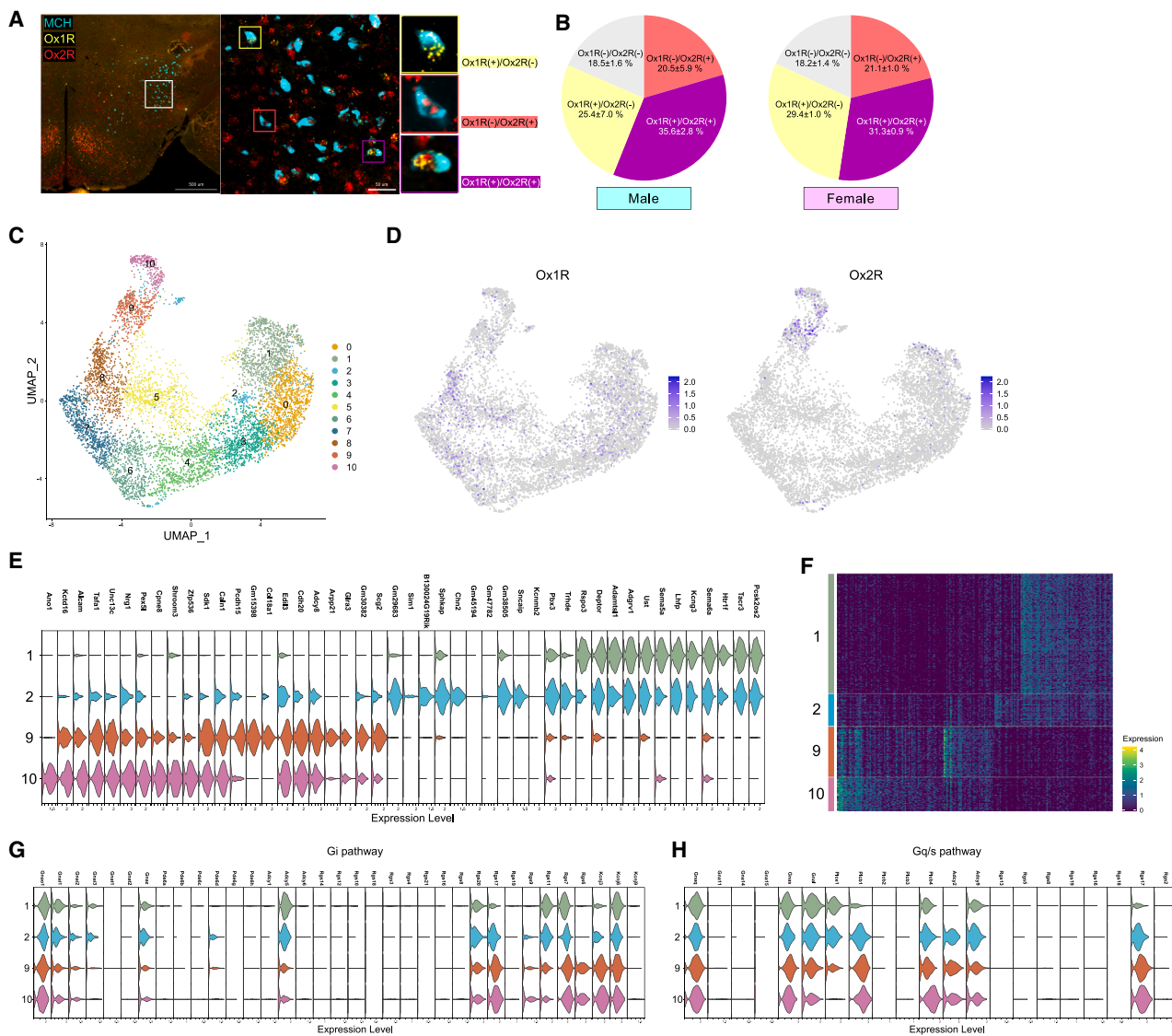


**Figure 1. Distribution of Ox2R in distinct sub-populations of MCH neurons**

- (A) *Pmch* (MCH), *Hcrtr1* (Ox1R), and *Hcrtr2* (Ox2R) mRNA expression in the hypothalamus detected by *in situ* hybridization.
- (B) Quantitative cell counts showing Ox1R and Ox2R expression in MCH neurons in 3 males (2,138 MCH neurons) and 3 females (1,843 MCH neurons).
- (C) Uniform manifold approximation and projection (UMAP) plots showing heterogeneous MCH neuron clusters based on single-nucleus sequencing from in *MCH-Cre; Isl-ZsGreen* mice (7,590 MCH neurons from 24 males and 23 females).
- (D) UMAP plots showing log-normalized expression of Ox1R (left) and Ox2R (right) in MCH neurons.
- (E) Violin plot representing the top 12 distinctive markers within the 4 sub-populations of Ox2R(+) MCH neurons in clusters 1, 2, 9, and 10.
- (F) Heatmap of cell clusters with marker genes of Ox2R(+) MCH neurons in clusters 1, 2, 9, and 10 as shown in Table S1B.
- (G) Violin plot showing marker genes related to Gi signaling.
- (H) Violin plot showing marker genes related to Gq/s signaling.

of *Hcrtr2* was selectively reduced in MCH neurons. Here, Ox2RΔMCH mice exhibited a significant 60%–70% reduction of mRNA for exon 2 exclusively in MCH neurons, whereas control (Ox2R *fl/fl*) littermates exhibited intact Ox2R expression in these neurons (Figures 3A–3C).

To investigate the role of Ox2R in sleep regulation, electroencephalography (EEG) and electromyography (EMG) recordings were conducted over 4 consecutive days following surgery

and a sufficient recovery and habituation period for the recording cable. Subsequently, we evaluated the EEG/EMG spectrograms in three stages: wake, REMS, and NREMS. In female Ox2RΔMCH mice, a fragmentation of NREMS events and a reduction in theta oscillation amplitude during REMS were observed compared to control mice (Figure 3D). The quantitative analysis of the four consecutive days demonstrated a significantly shortened mean duration of NREMS episodes

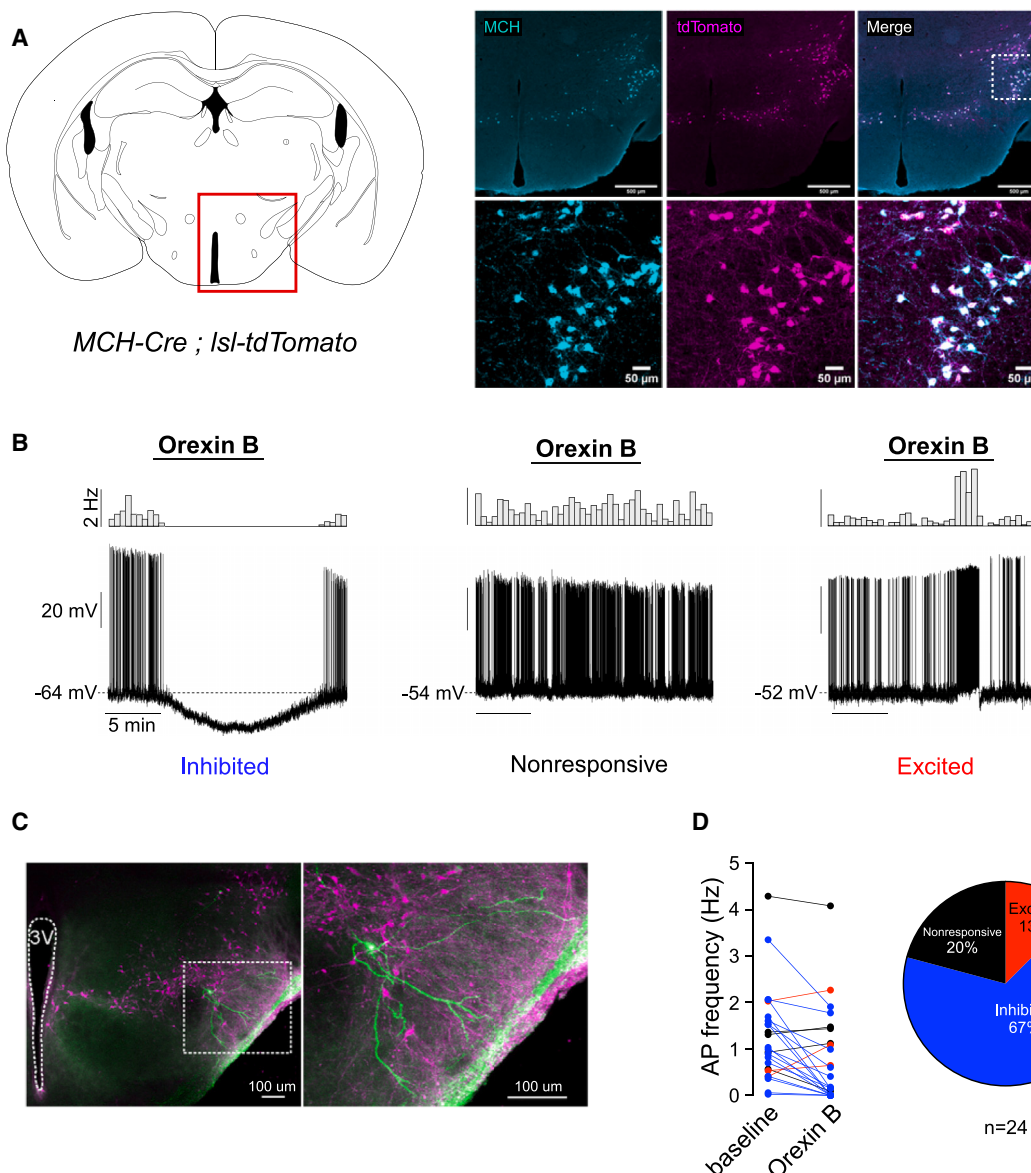


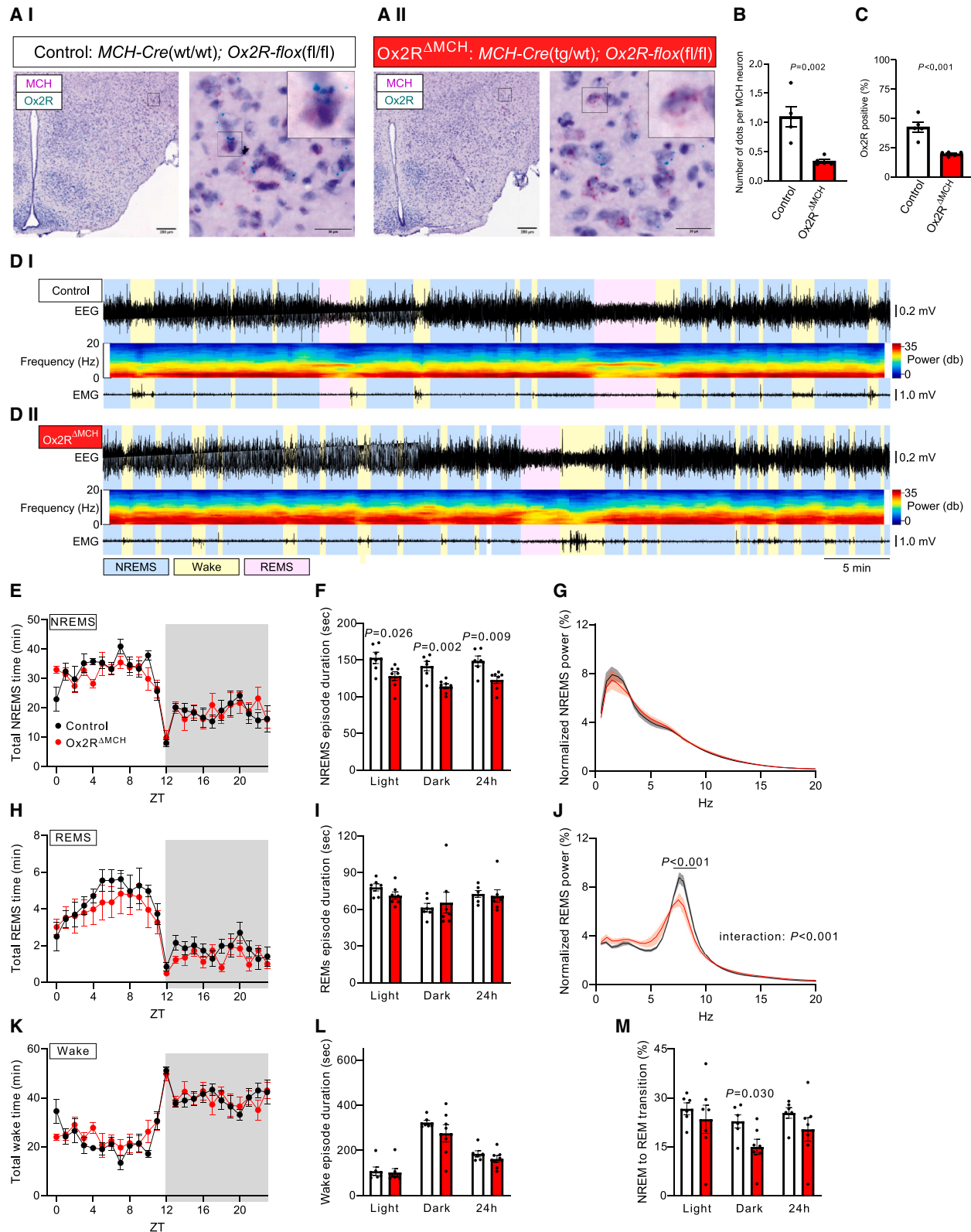
**Figure 2. Orexin B effects on MCH neurons in the lateral hypothalamus**

(A) *MCH-Cre; Isl-tdTomato* mice showing MCH-neuron-specific tdTomato expression.

(B–D) Orexin B effects on MCH neurons. Recordings were performed from tdTomato-labeled MCH neurons in acute brain slices of *MCH-Cre; Isl-tdTomato* mice in the perforated patch-clamp configuration to preserve intracellular signaling pathways. In all recordings, ionotropic GABAergic and glutamatergic synaptic input was pharmacologically blocked (see STAR Methods). The neurons were depolarized above the threshold at the beginning of the experiments. Orexin B was bath applied at 100 nM for 10 min. (B) Example recordings. Left: orexin B-inhibited neuron. Middle: neuron not responding to orexin B. Right: orexin B-excited neuron. Rate histograms (bin width: 30 s) (top) and the corresponding voltage recordings (bottom). Scale bars: frequency, 2 Hz; voltage, 20 mV; and time, 5 min. (C) 280 μm brain slice demonstrating the distribution of the MCH neurons in the lateral hypothalamus, including a recorded MCH neuron filled with biocytin after converting the perforated patch-clamp configuration to the whole-cell configuration. The neuron was double labeled with biocytin-streptavidin (green) and an anti-serum against tdTomato (magenta). (D) Summary graphs showing the number of individual neurons that were inhibited (blue) or excited (red) or did not react to orexin B (black) (for classification criteria, see STAR Methods and results). 3V, 3 ventricle.

(Figure 3F) and impaired theta oscillation amplitude during REMS (Figure 3J). Furthermore, the transition rate from NREMS to REMS was diminished during the dark period in female Ox2RΔMCH mice (Figures 3M and S3). These phenotypes were observed exclusively in female mice, with no significant

differences between Ox2RΔMCH and control male animals (Figure S4). Since MCH neuron activation induces a transition from NREMS to REMS, whereas inhibition impairs this transition and theta oscillation amplitude during REMS,<sup>18,40,41</sup> the observed impairment of REMS in Ox2RΔMCH mice is



(legend on next page)

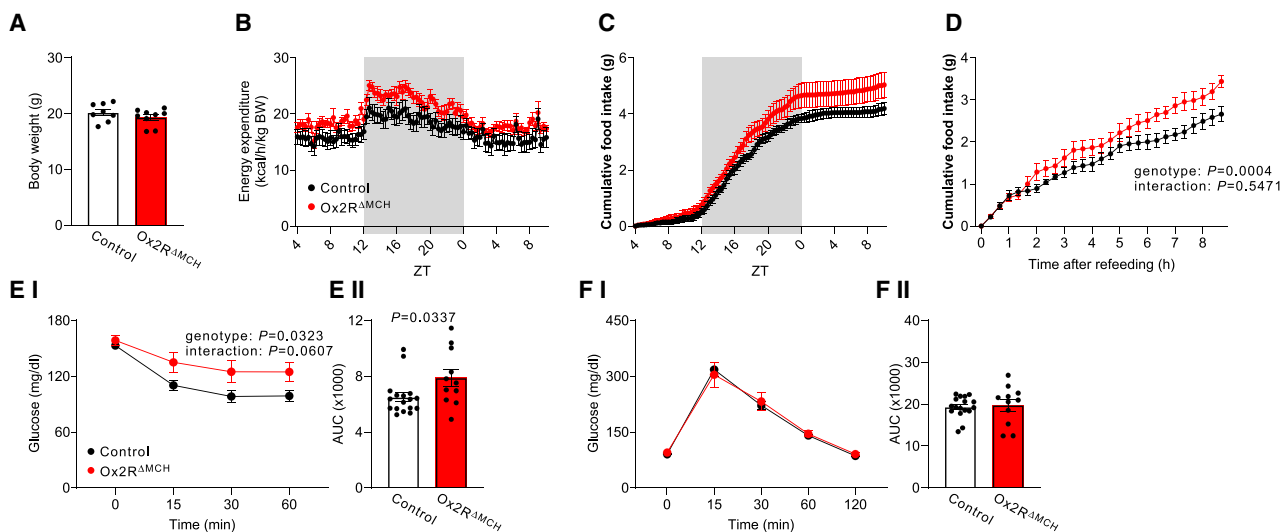


**Figure 4. Exaggerated refeeding and impaired insulin sensitivity upon Ox2R inactivation in MCH neurons in female mice**

(A) Body weight ( $n = 8$  vs. 9 mice).

(B and C) Energy expenditure (B) and cumulative food intake (C) measured over a 30-h period ( $n = 8$  vs. 9 mice).

(D) Cumulative food intake during refeeding period following a 16-h fasting ( $n = 8$  vs. 9 mice).

(E) Insulin tolerance test (E I) and area under the curve (AUC) (E II) for each mouse ( $n = 17$  vs. 11 mice).

(F) Glucose tolerance test (F I) following a 16-h fasting period and AUCs (F II) ( $n = 17$  vs. 11 mice).

Data are presented as mean  $\pm$  SEM.  $p$  value was calculated by two-way ANOVA followed by Bonferroni's test for (D) and (E I) and unpaired t test for (E II).

indicative of reduced activity of sleep-regulatory MCH neuron activity upon reduced Ox2R expression in the MCH neurons of these mice. Thus, the endogenous Ox2R might play a role in activating MCH neurons that regulate sleep. Moreover, observing a more pronounced sleep phenotype during the dark period than the light period is consistent with robust orexin signaling during the dark period.<sup>42,43</sup>

#### Exaggerated refeeding and impaired insulin sensitivity in female $Ox2R^{\Delta MCH}$ mice

Next, we investigated the consequences of MCH-neuron-restricted Ox2R inactivation on metabolic homeostasis. Female  $Ox2R^{\Delta MCH}$  mice exhibited unaltered body weight (Figure 4A) and no significant differences in steady-state energy expenditure and food intake compared to control mice (Figures 4B and 4C). However, during the refeeding period following a 16-h fasting, female  $Ox2R^{\Delta MCH}$  mice exhibited a significantly elevated food intake compared to the control mice (Figure 4D). Further-

more, the  $Ox2R^{\Delta MCH}$  mice showed an impairment in insulin sensitivity (Figures 4E and 4F). Similar to what was observed for altered sleep regulation, these metabolic phenotypes were exclusive to the females (Figure S5). In preceding studies, a subset of MCH neurons has been demonstrated to enhance food intake.<sup>44,45</sup> Intracerebroventricular injection of MCH peptides and overexpression of MCH have also been demonstrated to increase food intake and impair insulin resistance.<sup>1,19,20</sup> Conversely, ablation of MCH neurons has been shown to improve metabolic functions and results in body weight reduction.<sup>46,47</sup> Therefore, the impairment of metabolism in  $Ox2R^{\Delta MCH}$  mice is indicative of activation of metabolism-regulatory MCH neurons, indicating that Ox2R might play a role in inhibiting MCH neurons that regulate metabolism. In contrast to Ox2R, Ox1R inactivation in MCH neurons did not result in any notable differences between  $Ox1R^{\Delta MCH}$  and control mice regarding sleep and metabolism in male and female mice (Figures S6 and S7).

**Figure 3. REMS impairment upon Ox2R inactivation in MCH neurons in female mice**

(A) *Hcrtr2* (Ox2R) exon 2 and *Pmch* (MCH) mRNA expression in the control (A I) and  $Ox2R^{\Delta MCH}$  (A II) mice detected by *in situ* hybridization.

(B) Counts of Ox2R exon 2 mRNA dots per MCH neuron in 5 control and 5  $Ox2R^{\Delta MCH}$  mice.

(C) Cell counts of Ox2R exon 2 mRNA-positive MCH neurons in 5 control and 5  $Ox2R^{\Delta MCH}$  mice.

(D) EEG/EEG spectra and representative episodes of wakefulness (Wake), NREM sleep (NREMS), and REMS during 30 min of female control (D I) and  $Ox2R^{\Delta MCH}$  (D II) mice.

(E-G) Hourly time (E), mean duration of episodes (F), and EEG power spectra analysis (G) of NREMS.

(H-J) Hourly time (H), mean duration of episodes (I), and EEG power spectra analysis (J) of REMS.

(K and L) Hourly time (K) and mean duration of episodes (L) of Wake.

(M) Transition probability from NREM to REMS.

Data were measured over four days and averaged in zeitgeber (ZT) hours. Data are presented as mean  $\pm$  SEM.  $n = 6$  female mice for control and  $n = 7$  female mice for  $Ox2R^{\Delta MCH}$  in sleep measurement. Statistical  $p$  value was calculated by two-way ANOVA followed by Bonferroni's test for (J) and unpaired t test for (B), (C), (F), and (M).

**DISCUSSION**

OxR ligands orexin A and B regulate fundamental physiological functions via differential actions of widespread projections throughout the brain originating from the lateral hypothalamus. In preceding studies, orexin A administration to stimulate both Ox1R and Ox2R has revealed only excitatory responses in all brain regions and neuronal types examined.<sup>48,49</sup> Orexin B and Ox2R agonists also elicit excitatory responses in numerous neuronal cell types *in vivo* without inhibitory responses having been described in electrophysiological slice recordings,<sup>12–15</sup> including our previous reports on serotonergic neurons in the raphe nucleus.<sup>15</sup> Thus, current Ox2R studies, including the development of Ox2R agonists, have focused mainly on the role of Gq signaling and not much on the potential for a Gi-mediated inhibitory function, although this has been shown in *in vitro* studies.<sup>5,16</sup> The present study showed evidence of an inhibitory response via Ox2R signaling in MCH neurons by orexin B in acute brain slices. While previous studies have indicated that orexin A application on MCH neurons elicits primarily excitatory responses via Ox1R and 2R,<sup>39,50</sup> a more recent study has shown that less than 30% of recorded neurons exhibited excitatory responses and the overall average response did not change, suggesting the potential of an inhibitory response in a subset of MCH neurons by orexin A.<sup>25</sup> An inhibitory response might be induced by Ox2R, as indicated by inhibitory effects of orexin B application as identified in the present study.

Our snRNA sequencing studies showed that Ox2R(+) MCH neurons can be classified into several sub-populations that differ in their RNA expression, including that of GPCR-related mediators. It has been demonstrated that Ox2R protein modifications are diverse and dependent on the cells in which they are expressed, which suggests potentially variable functions of Ox2R as a GPCR.<sup>48,51</sup> Thus, the differential expression of Gi vs. Gq/s signaling components, even within molecularly heterogeneous MCH neurons, might alter the character of Ox2R signaling, resulting in both excitatory and inhibitory functions in specific MCH neurons. This notion is consistent with previous studies showing that MCH neurons can be classified into multiple molecularly and functionally distinct sub-populations. Single-cell calcium imaging experiments identified MCH neurons that are active during wakefulness and others that are active during REMS, which suggests that distinct MCH neurons regulate metabolism and sleep, respectively.<sup>41,52,53</sup> Single-cell/snRNA sequencing-based studies have identified *Cartpt* and *Tacr3* as markers of a sub-population of MCH neurons,<sup>29–32</sup> which we confirmed here. Recent studies have also demonstrated that electrophysiological properties differ between *Cartpt/Tacr3*-positive and -negative MCH neurons.<sup>32,33</sup> Altogether, these studies point toward a molecular and regulatory diversification of MCH neurons, the functional consequences of which remain not entirely clear at this point.

Several mechanisms maintain a balance between MCH and orexin neuron activity, such as an indirect inhibition via GABAergic neurons and an opposing glucose-dependent regulation between glucose-excited MCH neurons and glucose-inhibited orexin neurons.<sup>22–27</sup> The presumably inhibitory function of Ox2R in metabolism-regulating MCH neurons, which we sug-

gest in the present study, might be involved in balancing the activity of MCH and orexin neurons for metabolic homeostasis. On the other hand, functionally, our experiments indicate the possibility that a sub-population of Ox2R-expressing MCH neurons might activate sleep-regulating MCH neurons. In recent studies, specific sub-populations of orexin neurons have been reported to be active not only during wakefulness but also during REMS, indicating that a subset of orexin neurons might contribute to REMS homeostasis in addition to MCH neurons.<sup>54–56</sup> Thus, orexin signals might partially act to enforce REMS via Ox2R, which can activate sleep-regulating MCH neurons. Further supporting the notion of orexin neuron diversity, a recent study has already revealed the molecular heterogeneity and sub-populations of orexin neurons by single-cell RNA sequencing.<sup>57</sup>

Although *in vitro* studies have demonstrated that Ox2R can induce not only Gq-mediated excitatory but also Gi-mediated inhibitory effects, Ox2R-mediated inhibitory responses have not been reported *in vivo*. Our study focused on the heterogeneity of MCH neurons and revealed inhibitory, orexin B-, presumably Ox2R-mediated inhibitory effects in a subset of MCH neurons in slice recordings, and the metabolic phenotype of Ox2RΔMCH mice suggests an inhibitory function of Ox2R on a subset of MCH neurons *in vivo*. This finding might have the potential to expand the development and clinical application of pharmaceutical compounds targeting Ox2R. Interestingly, previous studies have shown that orexin A application can inhibit MCH neurons in slice recordings and that GABA<sub>A</sub> receptor blockade by gabazine can block the inhibitory effect of optogenetically stimulated orexin neurons on MCH neurons.<sup>25</sup> These data support a model where orexin A activates GABAergic interneurons, which in turn inhibit a subset of MCH neurons. In contrast, our study indicates that orexin B application can inhibit a substantial proportion of MCH neurons even in the presence of the GABA<sub>A</sub> receptor blocker picrotoxin. Therefore, we propose a dual mechanism of orexin-mediated MCH neuron inhibition, where orexin A, likely via Ox1R expressed in GABAergic interneurons, and orexin B, presumably via Ox2R expressed in MCH neurons, suppress the activity of subsets of MCH neurons. This model is also consistent with the lack of an obvious phenotype of mice lacking OxR1 in MCH neurons, as revealed by the present study.

Strikingly, the impairment of REMS and insulin sensitivity upon MCH-neuron-restricted OxR2 inactivation only manifests in female mice without any detectable phenotypical consequences in male mice. It has been previously shown that a number of factors induce sex differences in the orexin and MCH systems.<sup>58</sup> In particular, the pathway through which MCH neurons affect neurons in the nucleus accumbens (NAc) exhibits a sex difference, as MCH receptor 1 and estrogen receptor 1 are co-expressed in the NAc and estradiol alters the feeding-regulatory effect of MCH exclusively in females via the NAc.<sup>45</sup> In the present study, male and female mice exhibited comparable levels and ratios of Ox2R-expression in MCH neurons and similar electrophysiological responses to orexin B in MCH neurons, while Ox2RΔMCH mice showed female-specific phenotypes in sleep and metabolism. This suggests the possibility that the regions receiving Ox2R(+) MCH neuron projections might be regulated by sex

hormones, similar to what has been described for the NAc, resulting in the female-specific expression of phenotypes. Alternatively, Ox2R(+) MCH neuron projections might exhibit sex-specific differences. These aspects clearly deserve further studies.

### Limitations of the study

Although recent studies have shown the molecular<sup>29–32</sup> and regulatory<sup>41,52,53</sup> heterogeneity of MCH neurons, it is still unclear how these observations correspond functionally on the cellular level. Based on the phenotypes in sleep and metabolic control revealed in female Ox2RΔMCH mice, we can hypothesize that Ox2R mediates activatory signaling in sleep-regulating MCH neurons and inhibitory signaling in metabolism-regulating MCH neurons. However, this remains hypothetical because it is currently unknown which MCH neuron sub-population(s) regulate sleep or metabolism, respectively. Identification of molecular markers of MCH neuron sub-populations with inhibitory and excitatory responses to orexin B application by patch sequencing may provide an important approach for future studies.

Here, we identified an inhibitory response to orexin B from MCH neurons isolated from ionotropic GABAergic and glutamatergic input to minimize indirect modulatory effects. Since a recent study showed that a GABA<sub>A</sub> receptor block largely abolished the indirect inhibition of MCH neurons by orexin neuron stimulation,<sup>25</sup> it is tempting and straightforward to hypothesize a direct Ox2R- and Gi-mediated pathway in MCH neurons. Ultimately, defining the complete pathway from receptor signaling to target channel activation is essential.

### RESOURCE AVAILABILITY

#### Lead contact

Further information and requests for resources and reagents should be directed to and will be fulfilled by the lead contact, Jens Claus Brüning ([bruening@sf.mpg.de](mailto:bruening@sf.mpg.de)).

#### Materials availability

No unique reagents were generated in this study.

#### Data and code availability

- All data reported in this paper will be shared by the lead contact upon request.
- All original code has been deposited at <https://github.com/lsteuernagel/MCH-neurons-orexin> and <https://doi.org/10.5281/zenodo.14186803> and is publicly available as of the date of publication. DOIs are listed in the [key resources table](#).
- RNA sequencing data are available in the NCBI Gene Expression Omnibus under accession GEO: GSE281229. The accession numbers are listed in the [key resources table](#).
- Any additional information required to reanalyze the data reported in this paper is available from the [lead contact](#) upon request.

### ACKNOWLEDGMENTS

We thank Jens Albert, Pia Scholl, Christiane Schäfer, and Gregor Borghorst for their technical assistance. We are grateful to Christian Kukat and Kat Folz-Donahue (FACS & Imaging Core Facility, MPI for Biology of Aging) for support during the sorting of MCH neuron nuclei. This work was supported by Manpei Suzuki Diabetes Foundation fellowship and CECAD Senior Postdoc Grant (S.I.); DFG grants KL 762/7-1 (401832153) and KL 762/9-1 (505389599) and a Forum grant of the UoC Excellent Research Support Program (P.K.); and

European Research Council grant agreement ID 742106 and Federal Ministry of Education and Research (Germany)-German Center for Diabetes Research (DZD) ID 82DZD05D03 (J.C.B.).

### AUTHOR CONTRIBUTIONS

S.I. and J.C.B. designed the experiments. S.I., H.J., D.F., L.S., and C.H. performed the experiments. S.I., D.F., L.S., C.H., and P.K. performed the formal analysis. A.C.H. and F.T.W. developed the genetically modified mouse lines. S.I. and J.C.B. wrote the manuscript with input from all authors.

### DECLARATION OF INTERESTS

J.C.B. is a cofounder and shareholder of Cerapeutix and has received research funding through collaborations with Sanofi Aventis and Novo Nordisk and consultancy fees from Eli Lilly and Company and Novo Nordisk, which did not affect the content of this article.

### STAR METHODS

Detailed methods are provided in the online version of this paper and include the following:

- KEY RESOURCES TABLE
- EXPERIMENTAL MODEL AND STUDY PARTICIPANT DETAILS
  - Animal husbandry
  - Mouse lines
  - Generation of experimental mouse lines
- METHOD DETAILS
  - Electrode implantation surgery
  - Sleep recording and analysis
  - Indirect calorimetry
  - Insulin tolerance test (ITT)
  - Glucose tolerance test (GTT)
  - Nuclear isolation and single nucleus sorting for single nucleus sequencing
  - Single nucleus sequencing and analysis
  - Animals and brain slice preparation
  - Perforated patch clamp recordings
  - Single-neuron labeling
  - Perfusion for immunohistochemistry and RNA *in situ* hybridization
  - Immunohistochemistry
  - RNA *in situ* hybridization (RNAscope)
  - RNA *in situ* hybridization (BaseScope)
  - Microscopy and image processing
- QUANTIFICATION AND STATISTICAL ANALYSIS

### SUPPLEMENTAL INFORMATION

Supplemental information can be found online at <https://doi.org/10.1016/j.celrep.2025.115277>.

Received: September 24, 2024

Revised: November 5, 2024

Accepted: January 16, 2025

Published: February 12, 2025

### REFERENCES

1. Arrigoni, E., Chee, M.J.S., and Fuller, P.M. (2019). To eat or to sleep: That is a lateral hypothalamic question. *Neuropharmacology* **154**, 34–49.
2. Soya, S., and Sakurai, T. (2020). Evolution of Orexin Neuropeptide System: Structure and Function. *Front. Neurosci.* **14**, 691.
3. Dhafar, H.O., and BaHammam, A.S. (2022). Body Weight and Metabolic Rate Changes in Narcolepsy: Current Knowledge and Future Directions. *Metabolites* **12**, 1120. <https://doi.org/10.3390/metabo12111120>.

4. Sakurai, T., Amemiya, A., Ishii, M., Matsuzaki, I., Chemelli, R.M., Tanaka, H., Williams, S.C., Richardson, J.A., Kozlowski, G.P., Wilson, S., et al. (1998). Orexins and orexin receptors: a family of hypothalamic neuropeptides and G protein-coupled receptors that regulate feeding behavior. *Cellule* 92, 573–585.
5. Yin, J., Kang, Y., McGrath, A.P., Chapman, K., Sjodt, M., Kimura, E., Okabe, A., Koike, T., Miyahana, Y., Shimizu, Y., et al. (2022). Molecular mechanism of the wake-promoting agent TAK-925. *Nat. Commun.* 13, 2902.
6. Dauvilliers, Y., Mignot, E., Del Río Villegas, R., Du, Y., Hanson, E., Inoue, Y., Kadali, H., Koundourakis, E., Meyer, S., Rogers, R., et al. (2023). Oral Orexin Receptor 2 Agonist in Narcolepsy Type 1. *N. Engl. J. Med.* 389, 309–321.
7. Saitoh, T., and Sakurai, T. (2023). The present and future of synthetic orexin receptor agonists. *Peptides* 167, 171051.
8. Wang, W., Ranjan, A., Zhang, W., Liang, Q., MacMillan, K.S., Chapman, K., Wang, X., Chandrasekaran, P., Williams, N.S., Rosenbaum, D.M., and De Brabander, J.K. (2024). Novel orexin receptor agonists based on arene- or pyridine-fused 1,3-dihydro-2H-imidazole-2-imines. *Bioorg. Med. Chem. Lett.* 99, 129624.
9. Konofal, E. (2024). From past to future: 50 years of pharmacological interventions to treat narcolepsy. *Pharmacol. Biochem. Behav.* 241, 173804.
10. Zhu, Y., Miwa, Y., Yamanaka, A., Yada, T., Shibahara, M., Abe, Y., Sakurai, T., and Goto, K. (2003). Orexin receptor type-1 couples exclusively to pertussis toxin-insensitive G-proteins, while orexin receptor type-2 couples to both pertussis toxin-sensitive and -insensitive G-proteins. *J. Pharm. Sci.* 92, 259–266.
11. Kukkonen, J.P. (2016). OX2 orexin/hypocretin receptor signal transduction in recombinant Chinese hamster ovary cells. *Cell. Signal.* 28, 51–60.
12. Korotkova, T.M., Sergeeva, O.A., Eriksson, K.S., Haas, H.L., and Brown, R.E. (2003). Excitation of ventral tegmental area dopaminergic and nondoaminergic neurons by orexins/hypocretins. *J. Neurosci.* 23, 7–11.
13. Yamanaka, A., Tabuchi, S., Tsunematsu, T., Fukazawa, Y., and Tominaga, M. (2010). Orexin directly excites orexin neurons through orexin 2 receptor. *J. Neurosci.* 30, 12642–12652.
14. Yukitake, H., Fujimoto, T., Ishikawa, T., Suzuki, A., Shimizu, Y., Rikimaru, K., Ito, M., Suzuki, M., and Kimura, H. (2019). TAK-925, an orexin 2 receptor-selective agonist, shows robust wake-promoting effects in mice. *Pharmacol. Biochem. Behav.* 187, 172794.
15. Xiao, X., Yegiazaryan, G., Hess, S., Klemm, P., Sieben, A., Kleinridders, A., Morgan, D.A., Wunderlich, F.T., Rahmouni, K., Kong, D., et al. (2021). Orexin receptors 1 and 2 in serotonergic neurons differentially regulate peripheral glucose metabolism in obesity. *Nat. Commun.* 12, 5249.
16. Kukkonen, J.P. (2023). The G protein preference of orexin receptors is currently an unresolved issue. *Nat. Commun.* 14, 3162.
17. Saper, C.B., Chou, T.C., and Elmquist, J.K. (2002). The need to feed. *Neuron* 36, 199–211.
18. Bandaru, S.S., Khanday, M.A., Ibrahim, N., Naganuma, F., and Vetrivelan, R. (2020). Sleep-wake control by melanin-concentrating hormone (MCH) neurons: A review of recent findings. *Curr. Neurol. Neurosci. Rep.* 20, 55.
19. Ludwig, D.S., Tritos, N.A., Mastaitis, J.W., Kulkarni, R., Kokkotou, E., Elmquist, J., Lowell, B., Flier, J.S., and Maratos-Flier, E. (2001). Melanin-concentrating hormone overexpression in transgenic mice leads to obesity and insulin resistance. *J. Clin. Invest.* 107, 379–386.
20. Pereira-da-Silva, M., De Souza, C.T., Gasparetti, A.L., Saad, M.J.A., and Velloso, L.A. (2005). Melanin-concentrating hormone induces insulin resistance through a mechanism independent of body weight gain. *J. Endocrinol.* 186, 193–201.
21. Hausen, A.C., Ruud, J., Jiang, H., Hess, S., Varbanov, H., Kloppenburg, P., and Brüning, J.C. (2016). Insulin-Dependent Activation of MCH Neurons Impairs Locomotor Activity and Insulin Sensitivity in Obesity. *Cell Rep.* 17, 2512–2521.
22. Yamanaka, A., Beuckmann, C.T., Willie, J.T., Hara, J., Tsujino, N., Mieda, M., Tominaga, M., Yagami, K.I., Sugiyama, F., Goto, K., et al. (2003). Hypothalamic orexin neurons regulate arousal according to energy balance in mice. *Neuron* 38, 701–713.
23. Burdakov, D., Gerasimenko, O., and Verkhratsky, A. (2005). Physiological changes in glucose differentially modulate the excitability of hypothalamic melanin-concentrating hormone and orexin neurons *in situ*. *J. Neurosci.* 25, 2429–2433.
24. Kong, D., Vong, L., Parton, L.E., Ye, C., Tong, Q., Hu, X., Choi, B., Brüning, J.C., and Lowell, B.B. (2010). Glucose stimulation of hypothalamic MCH neurons involves K(ATP) channels, is modulated by UCP2, and regulates peripheral glucose homeostasis. *Cell Metab.* 12, 545–552.
25. Apergis-Schoute, J., Iordanidou, P., Faure, C., Jego, S., Schöne, C., Aitt-Aho, T., Adamantidis, A., and Burdakov, D. (2015). Optogenetic evidence for inhibitory signaling from orexin to MCH neurons via local microcircuits. *J. Neurosci.* 35, 5435–5441.
26. González, J.A., Iordanidou, P., Strom, M., Adamantidis, A., and Burdakov, D. (2016). Awake dynamics and brain-wide direct inputs of hypothalamic MCH and orexin networks. *Nat. Commun.* 7, 11395.
27. Viskaitis, P., Tesmer, A.L., Liu, Z., Karnani, M.M., Arnold, M., Donegan, D., Bracey, E., Grujic, N., Patriarchi, T., Peleg-Raibstein, D., and Burdakov, D. (2024). Orexin neurons track temporal features of blood glucose in behaving mice. *Nat. Neurosci.* 27, 1299–1308.
28. Cvetkovic, V., Brischoux, F., Jacquemard, C., Fellmann, D., Griffond, B., and Risold, P.-Y. (2004). Characterization of subpopulations of neurons producing melanin-concentrating hormone in the rat ventral diencephalon. *J. Neurochem.* 91, 911–919.
29. Mickelsen, L.E., Kolling, F.W., 4th, Chimileski, B.R., Fujita, A., Norris, C., Chen, K., Nelson, C.E., and Jackson, A.C. (2017). Neurochemical Heterogeneity Among Lateral Hypothalamic Hypocretin/Orexin and Melanin-Concentrating Hormone Neurons Identified Through Single-Cell Gene Expression Analysis. *eNeuro* 4, ENEURO.0013-17.2017. <https://doi.org/10.1523/ENEURO.0013-17.2017>.
30. Mickelsen, L.E., Bolisetty, M., Chimileski, B.R., Fujita, A., Beltrami, E.J., Costanzo, J.T., Naparstek, J.R., Robson, P., and Jackson, A.C. (2019). Single-cell transcriptomic analysis of the lateral hypothalamic area reveals molecularly distinct populations of inhibitory and excitatory neurons. *Nat. Neurosci.* 22, 642–656.
31. Jiang, H., Gallet, S., Klemm, P., Scholl, P., Folz-Donahue, K., Altmüller, J., Alber, J., Heilinger, C., Kukat, C., Loyens, A., et al. (2020). MCH Neurons Regulate Permeability of the Median Eminence Barrier. *Neuron* 107, 306–319.e9.
32. Fujita, A., Zhong, L., Antony, M.S., Chamiec-Case, E., Mickelsen, L.E., Kanoski, S.E., Flynn, W.F., and Jackson, A.C. (2021). Neurokinin B-Expressing Neurons of the Central Extended Amygdala Mediate Inhibitory Synaptic Input onto Melanin-Concentrating Hormone Neuron Subpopulations. *J. Neurosci.* 41, 9539–9560.
33. Miller, P.A., Williams-Ikenoba, J.G., Sankhe, A.S., Hoffe, B.H., and Chee, M.J. (2024). Neuroanatomical, electrophysiological, and morphological characterization of melanin-concentrating hormone cells coexpressing cocaine- and amphetamine-regulated transcript. *J. Comp. Neurol.* 532, e25588.
34. Chee, M.J.S., Arrigoni, E., and Maratos-Flier, E. (2015). Melanin-concentrating hormone neurons release glutamate for feedforward inhibition of the lateral septum. *J. Neurosci.* 35, 3644–3651.
35. Schneeberger, M., Tan, K., Nectow, A.R., Parolari, L., Caglar, C., Azevedo, E., Li, Z., Domingos, A., and Friedman, J.M. (2018). Functional analysis reveals differential effects of glutamate and MCH neuropeptide in MCH neurons. *Mol. Metab.* 13, 83–89.
36. Sankhe, A.S., Bordeleau, D., Alfonso, D.I.M., Wittman, G., and Chee, M.J. (2023). Loss of glutamatergic signalling from MCH neurons reduced anxiety-like behaviours in novel environments. *J. Neuroendocrinol.* 35, e13222.

37. Reuveny, E., Slesinger, P.A., Inglese, J., Morales, J.M., Iñiguez-Lluhi, J.A., Lefkowitz, R.J., Bourne, H.R., Jan, Y.N., and Jan, L.Y. (1994). Activation of the cloned muscarinic potassium channel by G protein beta gamma subunits. *Nature* 370, 143–146.
38. Masuho, I., Balaji, S., Muntean, B.S., Skamangas, N.K., Chavali, S., Tesmer, J.J.G., Babu, M.M., and Martemyanov, K.A. (2020). A global map of G protein signaling regulation by RGS proteins. *Cell* 183, 503–521.e19.
39. van den Pol, A.N., Acuna-Goycolea, C., Clark, K.R., and Ghosh, P.K. (2004). Physiological properties of hypothalamic MCH neurons identified with selective expression of reporter gene after recombinant virus infection. *Neuron* 42, 635–652.
40. Jego, S., Glasgow, S.D., Herrera, C.G., Ekstrand, M., Reed, S.J., Boyce, R., Friedman, J., Burdakov, D., and Adamantidis, A.R. (2013). Optogenetic identification of a rapid eye movement sleep modulatory circuit in the hypothalamus. *Nat. Neurosci.* 16, 1637–1643.
41. Izawa, S., Chowdhury, S., Miyazaki, T., Mukai, Y., Ono, D., Inoue, R., Ohmura, Y., Mizoguchi, H., Kimura, K., Yoshioka, M., et al. (2019). REM sleep-active MCH neurons are involved in forgetting hippocampus-dependent memories. *Science* 365, 1308–1313.
42. Justinussen, J.L., Holm, A., and Kornum, B.R. (2015). An optimized method for measuring hypocretin-1 peptide in the mouse brain reveals differential circadian regulation of hypocretin-1 levels rostral and caudal to the hypothalamus. *Neuroscience* 310, 354–361.
43. Taheri, S., Sunter, D., Dakin, C., Moyes, S., Seal, L., Gardiner, J., Rossi, M., Ghatei, M., and Bloom, S. (2000). Diurnal variation in orexin A immunoreactivity and prepro-orexin mRNA in the rat central nervous system. *Neurosci. Lett.* 279, 109–112.
44. Noble, E.E., Hahn, J.D., Konanur, V.R., Hsu, T.M., Page, S.J., Cortella, A.M., Liu, C.M., Song, M.Y., Suarez, A.N., Szujewski, C.C., et al. (2018). Control of Feeding Behavior by Cerebral Ventricular Volume Transmission of Melanin-Concentrating Hormone. *Cell Metab.* 28, 55–68.e7.
45. Terrill, S.J., Subramanian, K.S., Lan, R., Liu, C.M., Cortella, A.M., Noble, E.E., and Kanoski, S.E. (2020). Nucleus accumbens melanin-concentrating hormone signaling promotes feeding in a sex-specific manner. *Neuropharmacology* 178, 108270.
46. Whiddon, B.B., and Palmiter, R.D. (2013). Ablation of neurons expressing melanin-concentrating hormone (MCH) in adult mice improves glucose tolerance independent of MCH signaling. *J. Neurosci.* 33, 2009–2016.
47. Izawa, S., Yoneshiro, T., Kondoh, K., Nakagiri, S., Okamatsu-Ogura, Y., Terao, A., Minokoshi, Y., Yamanaka, A., and Kimura, K. (2022). Melanin-concentrating hormone-producing neurons in the hypothalamus regulate brown adipose tissue and thus contribute to energy expenditure. *J. Physiol.* 600, 815–827.
48. Leonard, C.S., and Kukkonen, J.P. (2014). Orexin/hypocretin receptor signalling: a functional perspective. *Br. J. Pharmacol.* 171, 294–313.
49. Chen, Q., de Lecea, L., Hu, Z., and Gao, D. (2015). The hypocretin/orexin system: an increasingly important role in neuropsychiatry: The hypocretin/orexin system in neuropsychiatry. *Med. Res. Rev.* 35, 152–197.
50. Li, Y., and van den Pol, A.N. (2006). Differential target-dependent actions of coexpressed inhibitory dynorphin and excitatory hypocretin/orexin neuropeptides. *J. Neurosci.* 26, 13037–13047.
51. Kukkonen, J.P., and Turunen, P.M. (2021). Cellular signaling mechanisms of hypocretin/orexin. *Front. Neurol. Neurosci.* 45, 91–102.
52. Blanco-Centurion, C., Luo, S., Spergel, D.J., Vidal-Ortiz, A., Oprisan, S.A., Van den Pol, A.N., Liu, M., and Shiromani, P.J. (2019). Dynamic Network Activation of Hypothalamic MCH Neurons in REM Sleep and Exploratory Behavior. *J. Neurosci.* 39, 4986–4998.
53. Sun, Y., and Liu, M. (2020). Hypothalamic MCH Neuron Activity Dynamics during Cataplexy of Narcolepsy. *eNeuro* 7, ENEURO.0017-20.2020. <https://doi.org/10.1523/ENEURO.0017-20.2020>.
54. Feng, H., Wen, S.-Y., Qiao, Q.-C., Pang, Y.-J., Wang, S.-Y., Li, H.-Y., Cai, J., Zhang, K.-X., Chen, J., Hu, Z.-A., et al. (2020). Orexin signaling modulates synchronized excitation in the sublaterodorsal tegmental nucleus to stabilize REM sleep. *Nat. Commun.* 11, 3661.
55. Ito, H., Fukatsu, N., Rahaman, S.M., Mukai, Y., Izawa, S., Ono, D., Kilduff, T.S., and Yamanaka, A. (2023). Deficiency of orexin signaling during sleep is involved in abnormal REM sleep architecture in narcolepsy. *Proc. Natl. Acad. Sci. USA* 120, e2301951120.
56. Feng, H., Qiao, Q.-C., Luo, Q.-F., Zhou, J.-Y., Lei, F., Chen, Y., Wen, S.-Y., Chen, W.-H., Pang, Y.-J., Hu, Z.-A., et al. (2024). Orexin Neurons to Sublaterodorsal Tegmental Nucleus Pathway Prevents Sleep Onset REM Sleep-Like Behavior by Relieving the REM Sleep Pressure. *Research* 7, 355.
57. Li, S.-B., Damonte, V.M., Chen, C., Wang, G.X., Kebschull, J.M., Yamaguchi, H., Bian, W.-J., Purmann, C., Pattni, R., Urban, A.E., et al. (2022). Hyperexcitable arousal circuits drive sleep instability during aging. *Science* 375, eabh3021.
58. Gao, X.-B., and Horvath, T.L. (2022). From molecule to behavior: Hypocretin/orexin revisited from a sex-dependent perspective. *Endocr. Rev.* 43, 743–760.
59. Löhr, H., Hess, S., Pereira, M.M.A., Reinoß, P., Leibold, S., Schenkel, C., Wunderlich, C.M., Kloppenburg, P., Brünning, J.C., and Hammerschmidt, M. (2018). Diet-Induced Growth Is Regulated via Acquired Leptin Resistance and Engages a Pomc-Somatostatin-Growth Hormone Circuit. *Cell Rep.* 23, 1728–1741.
60. Zheng, G.X.Y., Terry, J.M., Belgrader, P., Ryvkin, P., Bent, Z.W., Wilson, R., Ziraldo, S.B., Wheeler, T.D., McDermott, G.P., Zhu, J., et al. (2017). Massively parallel digital transcriptional profiling of single cells. *Nat. Commun.* 8, 14049.
61. Madisen, L., Zwingman, T.A., Sunkin, S.M., Oh, S.W., Zariwala, H.A., Gu, H., Ng, L.L., Palmiter, R.D., Hawrylycz, M.J., Jones, A.R., et al. (2010). A robust and high-throughput Cre reporting and characterization system for the whole mouse brain. *Nat. Neurosci.* 13, 133–140.
62. Hao, Y., Hao, S., Andersen-Nissen, E., Mauck, W.M., 3rd, Zheng, S., Butler, A., Lee, M.J., Wilk, A.J., Darby, C., Zager, M., et al. (2021). Integrated analysis of multimodal single-cell data. *Cell* 184, 3573–3587.e29.
63. Steuernagel, L., Lam, B.Y.H., Klemm, P., Dowsett, G.K.C., Bauder, C.A., Tadross, J.A., Hitschfeld, T.S., Del Rio Martin, A., Chen, W., de Solis, A.J., et al. (2022). HypoMap—a unified single-cell gene expression atlas of the murine hypothalamus. *Nat. Metab.* 4, 1402–1419.
64. Lotfollahi, M., Naghipourfar, M., Luecken, M.D., Khajavi, M., Büttner, M., Wagenstetter, M., Avsec, Ž., Gayoso, A., Yosef, N., Interlandi, M., et al. (2022). Mapping single-cell data to reference atlases by transfer learning. *Nat. Biotechnol.* 40, 121–130.
65. Hess, S., Wratil, H., and Kloppenburg, P. (2023). Perforated Patch Clamp Recordings in ex vivo Brain Slices from Adult Mice. *Bio. Protoc.* 13, e4741.

## STAR★METHODS

### KEY RESOURCES TABLE

REAGENT or RESOURCE	SOURCE	IDENTIFIER
<b>Antibodies</b>		
Anti-MCH antibody produced in rabbit	Sigma-Aldrich	Cat# M8440; RRID:AB_260690
dsRed Polyclonal Antibody	Takara Bio	Cat# 632496; RRID:AB_10013483
Goat anti-Rabbit IgG (H + L) Cross-Adsorbed Secondary Antibody, Alexa Fluor™ 647	Invitrogen	Cat# A-21244; RRID:AB_2535812
Alexa Fluor 488-AffiniPure Goat Anti-Rabbit IgG (H + L) (min X Hu,Ms,Rat Sr Prot)	Jackson ImmunoResearch Labs	Cat# 111-545-144; RRID:AB_2338052
<b>Chemicals, peptides, and recombinant proteins</b>		
Buprenorphine	Bayer	PZN 01498870
Meloxicam	Boehringer Ingelheim	PZN 07578423
Tramal	Grünenthal GmbH	Cat#95005446
Isoflurane	CP-pharma	Cat#1214
Isoflurane	AbbVie	Cat#B506
20% glucose	B. Braun	N/A
Human Insulin	Eli Lilly	Cat#HP8804
EZ PREP buffer	Sigma	Cat#D8938
DAPI	Thermo Fisher Scientific	Cat#62248
Picrotoxin	Sigma-Aldrich	Cat#P1675
DL-2-amino-5-phosphonopentanoic acid	Biotrend	Cat#BN0086
6-cyano-7-nitroquinoxaline-2,3-dione	Sigma-Aldrich	Cat#C127
Amphotericin B	Sigma-Aldrich	Cat#A4888
Biocytin	Sigma-Aldrich	Cat#B4261
DMSO	Sigma-Aldrich	Cat#D8418
Orexin B	Sigma-Aldrich	Cat#O6262
Roti-Histofix	Carl Roth	Cat#P0873
Entellan	Sigma-Aldrich	Cat#107960
Vectashield Antifade Mounting Medium	Vector Laboratories	Cat#H-1200
VectaMount mounting media	Vector Laboratories	Cat#H-5000
Haematoxylin	Vector Laboratories	Cat#H-3404
RNAscope HybEZ hybridization system	ACD bio/Bio-Techne	Cat#321462
RNAscope Protease Plus	ACD bio/Bio-Techne	Cat#322331
RNAscope Target Retrieval	ACD bio/Bio-Techne	Cat#322000
Opal 520 Fluorophore	Akoya Bioscience	Cat#FP1487001KT
Opal 570 Fluorophore	Akoya Bioscience	Cat#FP1488001KT
Opal 690 Fluorophore	Akoya Bioscience	Cat#FP1497001KT
<b>Critical commercial assays</b>		
Super-Bond Universal Kit	SUN MEDICAL	N/A
REPAIRSIN	GC	N/A
Chromium Single Cell 3' Reagent Kits v3	10x Genomics	Cat#1000092 and 1000074
RNAscope Multiplex Fluorescent Detection kit v2	ACD bio/Bio-Techne	Cat#323100
RNAscope Hcrtr1 probe	ACD bio/Bio-Techne	Cat#466631-C2
RNAscope Hcrtr2 probe	ACD bio/Bio-Techne	Cat#581631-C3

(Continued on next page)

**Continued**

REAGENT or RESOURCE	SOURCE	IDENTIFIER
RNAscope Pmch probe	ACD bio/Bio-Techne	Cat#478721-C4
BaseScope Duplex Detection Kit	ACD bio/Bio-Techne	Cat#323800
BaseScope Pmch probe	ACD bio/Bio-Techne	Cat#890511-C2
<b>Deposited data</b>		
Github Repository	This study	<a href="https://github.com/Isteuernagel/MCH-neurons-orexin">https://github.com/Isteuernagel/MCH-neurons-orexin</a>
Zenodo DOI	This study	<a href="https://doi.org/10.5281/zenodo.14186803">https://doi.org/10.5281/zenodo.14186803</a>
GEO Accession	This study	<a href="https://www.ncbi.nlm.nih.gov/geo/query/acc.cgi?acc=GSE281229">https://www.ncbi.nlm.nih.gov/geo/query/acc.cgi?acc=GSE281229</a>
<b>Experimental models: Organisms/strains</b>		
C57BL/6N	Charles River	Strain Code: 027
MCH-Cre	Kong et al. <sup>24</sup>	N/A
R26- <i>Isl</i> -ZsGreen	Löhr et al. <sup>59</sup>	N/A
R26- <i>Isl</i> -tdTomato	Jackson Laboratory	Strain Code: 007905
Ox1R fl/fl	Xiao et al. <sup>15</sup>	N/A
Ox2R fl/fl	Xiao et al. <sup>15</sup>	N/A
<b>Oligonucleotides</b>		
Custom-designed Base scope probe targeting the region 615–948 of the <i>Hcrtr1</i> transcript	ACD bio/Bio-Techne	N/A
Custom-designed Base scope probe targeting the region 413–502 of the <i>Hcrtr2</i> transcript	ACD bio/Bio-Techne	N/A
<b>Software and algorithms</b>		
SleepSignRecorder	Kissei Comtec	N/A
SleepSign3	Kissei Comtec	N/A
10x Genomics Cell Ranger	Zheng et al. <sup>60</sup>	<a href="https://www.10xgenomics.com/jp/support/software/cell-ranger/latest">https://www.10xgenomics.com/jp/support/software/cell-ranger/latest</a>
R Studio	The R Foundation for Statistical Computing, Institute for Statistics and Mathematics, University of Economics and Business, Austria	<a href="https://www.r-project.org">https://www.r-project.org</a>
PatchMaster, version 2x90	HEKA Elektronik	N/A
Spike 2, version 7.01	Cambridge Electronic Design	N/A
Igor Pro, version 6.37	Wavemetrics	N/A
Prism 9 for macOS, v 9.5.1	Graphpad	N/A
Prism 10, v 10.0.2	Graphpad	N/A
Fiji/ImageJ v2.14.0	<a href="https://imagej.net&gt;Welcome">https://imagej.net&gt;Welcome</a>	<a href="https://imagej.nih.gov/ij/download.html">https://imagej.nih.gov/ij/download.html</a>
Affinity Designer, Ver. 1.10.8	Serif Ltd	N/A
<b>Other</b>		
Normal Chow Diet (ssniff R/M-H Phytoestrogenarm)	Ssniff Spezialdiäten	Cat#V1554
Phenomaster	TSE Systems	<a href="https://www.tse-systems.com/service/phenomaster/">https://www.tse-systems.com/service/phenomaster/</a>
High sensitivity amplifier	Miyuki-Giken	Cat#AB-611JMG
SuperFrost Plus Gold slides	Thermo Fisher	Cat#K5800AMNT72
BD FACSaria Illu	BD Bioscience	N/A
Contour XT	Bayer Healthcare	N/A
Borosilicate glass	Science Products	Cat#GB150-8P
Vertical pipette puller	Narishige	Cat#PP-830
EPC10 patch-clamp amplifier	HEKA Elektronik	N/A

(Continued on next page)

**Continued**

REAGENT or RESOURCE	SOURCE	IDENTIFIER
Confocal microscope	Leica	Cat#SP-8
Vibration microtome	Leica	Cat#VT1200
Research Cryostat	Leica	Cat#CM3050-S
Slide scanner	Olympus	Cat#VS200

## EXPERIMENTAL MODEL AND STUDY PARTICIPANT DETAILS

### Animal husbandry

All animal procedures were conducted in compliance with protocols approved by local government authorities (Bezirksregierung Köln) and were in accordance with NIH guidelines. Mice breeding and maintenance was permitted by the Department for Environment and Consumer Protection – Veterinary Section, Köln, North Rhine-Westphalia, Germany. Mice were housed in individually ventilated cages (IVCs) within a controlled environment at 22°C–24°C and a 12-h light/12-h dark cycle. Mice were checked daily to verify animal health and the health status monitoring of the animal facility was performed quarterly every year. Mice were housed in groups of not more than 5 mice per cage after weaning. Animals received *ad libitum* access standard rodent chow (ssniff V1554, 59494 Soest, Germany) and water. All the mouse lines generated in the paper were maintained in house on a C57BL/6N background. Mice were age-matched between experimental groups for both males and females. Littermates were assigned to the experimental groups, with OxR1fl/fl and OxR2fl/fl mice served as controls for Ox1RΔMCH and Ox2RΔMCH mice, respectively.

### Mouse lines

#### C57BL/6N

This mouse line was obtained from Charles River, Germany.

#### MCH-Cre

This line was kindly provided by the lab of Bradford B. Lowell.<sup>24</sup>

#### R26-*Isl*-ZsGreen

This mouse line was generated in our facility and described previously.<sup>59</sup> In the mice, a *loxP* site-flanked *neo* stop cassette prevents expression of 2A-NLS-ZsGreen from the CAG promoter.

#### R26-*Isl*-tdTomato

Ai9 (B6; 129S6-Gt(ROSA)26Sortm9(CAG-tdTomato)Hze/J, 007905) line<sup>61</sup> was obtained from Jackson laboratory.

#### Ox1R fl/fl

This mouse line was generated in our facility and described previously.<sup>15</sup> The mice possess *loxP* sites flanking exon 4, 5 and 6 of the Ox1R gene (*Hcrtr1*).

#### Ox2R fl/fl

This mouse line was generated in our facility and described previously.<sup>15</sup> The mice possess *loxP* sites flanking exon 2 of the Ox2R gene (*Hcrtr2*).

### Generation of experimental mouse lines

#### MCH-Cre; *Isl*-ZsGreen

Heterozygous MCH-Cre mice were bred to homozygous R26-*Isl*-ZsGreen mice to generate MCH-Cre; *Isl*- ZsGreen mice as experimental animals.

#### MCH-Cre; *Isl*-tdTomato

Heterozygous MCH-Cre mice were bred to homozygous R26-*Isl*-tdTomato mice to generate MCH-Cre; *Isl*-tdTomato mice as experimental animals.

#### Ox1RΔMCH

Ox1R fl/fl animals were crossed with MCH-Cre mice for MCH neuron specific Ox1R inactivation.

#### Ox2RΔMCH

Ox2R fl/fl animals were crossed with MCH-Cre mice for MCH neuron specific Ox2R inactivation.

## METHOD DETAILS

### Electrode implantation surgery

Mice received 1 mg/mL of tramadol in drinking water 2 days before the surgeries. On the day of surgery, mice were anesthetized with isoflurane and a bolus of buprenorphine (0.1 mg/kg BW) was given (i.p.) to reduce pain. Two stainless screws were implanted on the skull (AP = +1.5 mm; ML = 1.5 and AP = -2.7 mm; ML = 2.3 mm from bregma) to record electroencephalogram (EEG), and two copper

wires (209–4811, RS PRO) were inserted on either side of the nuchal muscle to record electromyogram (EMG). All screws and wires were secured to the connector pins using Super-Bond (Super-Bond C&B, Sun Medical) and dental cement (REPAIRSIN, GC). Mice received a bolus of meloxicam (5 mg/kg BW, s.c.), and tramadol in drinking water for 3 days after surgeries, to relieve pain.

### Sleep recording and analysis

After recovery period from surgery at least for 7 days in their home cage and habituation period for 4 days in the recording conditions with cable connection, EEG and EMG recordings were conducted with amplification (AB-611JMG, Miyuki Giken), filtering (EEG, 0.5–30 Hz; EMG, 15–128 Hz), and digitization at a sampling rate of 128 Hz using SleepSignRecorder (Kissei Comtec). To determine vigilance states, EEG and EMG signals were scored in 10 s epochs and classified as wakefulness, NREM sleep, or REM sleep with SleepSign3 software (Kissei Comtec) by an experimenter who was blind to the genotype and experimental condition. Spectral analysis of the EEG was performed by fast Fourier transform to show power spectra profiles over a 0.5–20 Hz window with a 0.5 Hz resolution. An average EEG spectral profile was calculated from the EEG power densities in each frequency bin and normalized to total frequency range (0.5–20 Hz).

### Indirect calorimetry

Indirect calorimetry was performed using the indirect calorimetry system PhenoMaster (TSE Systems). Mice were single housed in calorimetric cages for three days prior to data acquisition to adapt them to the systems' food and water dispensers. During measurement, all parameters were measured continuously and simultaneously every 20 min. Food and water were provided *ad libitum* in the appropriate devices, and food intake was measured by the integrated automatic instruments. For the analysis of food intake following fasting and refeeding, the bedding was changed, and food hoppers were removed overnight for 16 hr. Subsequently, food hoppers were reinstated in the cage at ZT 4 the following day, and food intake was monitored.

### Insulin tolerance test (ITT)

Insulin tolerance tests (ITTs) were performed in random fed mice at ZT 3. Prior to starting the experiment, mice were transferred to a new cage and food was removed during the duration of the experiment. After measurement of the basal blood glucose concentrations, mice received an i.p. injection of 0.75U/kg body weight of human insulin (HP8804, Huminsulin Normal 100, Lilly) diluted in 0.9% saline. Blood glucose concentrations were measured from whole venous blood using an automatic glucose monitor (Contour XT, Bayer Healthcare) and measured at 15, 30 and 60 min post injection. Glucose levels at each timepoint represent the mean of at least two repetitive measurements using two independent glucose monitors.

### Glucose tolerance test (GTT)

Glucose tolerance tests (GTGs) were performed in 16 h fasted mice at ZT 3. To subject mice to an overnight fasting period, animals were transferred to a new cage and food was removed at ZT 11 the day before the experiment. After measurement of the basal blood glucose concentrations, mice received an i.p. injection of 2 g/kg body weight glucose (20% glucose solution, B. Braun). Blood glucose concentrations were measured from whole venous blood using an automatic glucose monitor (Contour XT, Bayer Healthcare) and measured at 15, 30, 60 and 120 min post injection. Glucose levels at each timepoint represent the mean of at least two repetitive measurements using two independent glucose monitors.

### Nuclear isolation and single nucleus sorting for single nucleus sequencing

The nuclear isolation and single nucleus sorting was performed according to a protocol described elsewhere.<sup>31</sup> Hypothalami of *MCH-Cre; Isl-ZsGreen* mice were dissected and frozen in liquid nitrogen immediately. Further, collected tissues were stored in –80°C until use. On single nuclei preparation day, individual hypothalami tissue were lysed in 1mL of ice-cold EZ PREP buffer (D8938, Sigma). The tissue was homogenized with a glass dounce, twice at 250 rpm and 12 times at 1000 rpm and incubated on ice for 5 min. Nuclei were centrifuged at 500 g, 5 min after addition of 4 mL of nuclear lysis buffer and incubated on ice for 5 min. The supernatant was discarded, and the pellet was resuspended in 4 mL nucleus suspension buffer (NSB, 1x PBS, 0.01% BSA, and 0.1% RNase inhibitor (Clontech). Nuclei were centrifuged at 500 g for 2 min. The supernatant was discarded and isolated nuclei were resuspended in 300 µL NSB and then filtered through a 30 µm cell strainer into sorting tubes for flow cytometry sorting on a BD FACSaria Illu.

Nuclei suspension was stained with DAPI (1:1000, 62248, Thermo Fisher Scientific) as nuclear marker. ZsGreen positive nuclei + DAPI positive nuclei were collected as MCH neuron nuclei. A FACSaria Illu was used for gating and sorting nuclei. Single nuclei were identified based on side scatter (SSC-A) and DAPI fluorescence (area versus width). ZsGreen fluorescence was detected with 488 nm excitation and 530 nm emission. Sorting was performed at 4°C with a 70 µm nozzle. Sorted ZsGreen positive nuclei were collected into 1xPBS buffer with 0.04% BSA for 10x genomics single cell sequencing.

### Single nucleus sequencing and analysis

For snRNA library construction, Chromium Single Cell 3' Reagent Kits v3 were used.

Single nucleus suspensions in 1xPBS containing 0.04% BSA (700–1200 nuclei/µl) were checked for viability which should ideally exceed 75% and be free of debris and cell aggregates. To achieve single cell resolution, the cells were delivered at a limiting dilution,

such that the majority (~90–99%) of generated GEMs contains no cell, while the remainder largely contain a single cell. Upon dissolution of the Single Cell 3' Gel Bead in a GEM, primers containing (i) an Illumina R1 sequence (read 1 sequencing primer), (ii) a 16 bp 10x Barcode, (iii) a 12 bp Unique Molecular Identifier (UMI) and (iv) a poly-dT primer sequence were released and mixed with cell lysate and Master Mix. Incubation of the GEMs produced barcoded, full-length cDNA from poly-adenylated mRNA. After incubation, the GEMs were broken and the pooled fractions were recovered. Silane magnetic beads were used to remove leftover biochemical reagents and primers from the post GEM reaction mixture. Full-length, barcoded cDNA was amplified by PCR to generate sufficient mass for library construction. Enzymatic fragmentation and size selection were used to optimize the cDNA amplicon size prior to library construction. R1 (read 1 primer sequence) were added to the molecules during GEM incubation. P5, P7, a sample index and R2 (read 2 primer sequence) were added during library construction via End Repair, A-tailing, Adaptor Ligation and PCR. The final libraries contained the P5 and P7 primers used in Illumina bridge amplification. We allocated Illumina NovaSeq6000 S2 flow cells to sequence with the first read 28nt (cell specific barcode and UMI) and generated with the second read 90nt 3'mRNA transcriptome data. Library preparation and sequencing was performed by the Cologne Center for Genomics.

Two single nucleus 10x samples were obtained. Raw sequence reads were mapped and genes counted based on the GRCm38 reference genome assembly (mm10-2020-A) using 10x Genomics Cell Ranger (v6.1.2).<sup>60</sup> Cells were filtered to have at least 800 unique molecular identifiers, 500 unique genes and a rate of mitochondrial RNA below 5%. The remaining 11,242 cells were processed using the Seurat R package (v4.4.0) using a pipeline with default settings for variable feature detection (1000 highly variable features), PCA (50 PCs), UMAP calculation and Louvain clustering (resolution = 1) for cluster detection (v4.3.0).<sup>62</sup> We used our previously described reference atlas HypoMap<sup>63</sup> and the scArches<sup>64</sup> algorithm to transfer labels for all hypothalamic cell types onto the MCH-dataset. Each Louvain cluster was annotated using the HypoMap label with the highest percentage of cells in that cluster and we subsequently removed all clusters with a high percentage of non-neuronal or non-MCH neuron labels. We re-processed the remaining 7,590 MCH-neurons using the same Seurat pipeline with a lower highly variable feature number (500) and Louvain resolution (0.8), resulting in 10 subclusters. The Seurat function *FindMarkers* was used to detect marker genes between all subclusters or specifically between Ox1R- and 2R expressing-clusters defined based on the percentage of cells expressing *Hcrtr1* and *Hcrtr2* in each of the 10 subclusters. Figures were generated using the Seurat and ggplot2 (v3.4.4) R packages. Marker genes shown in Figures were selected based on log2-foldchange. Gi and Gq related genes were selected from existing literature.<sup>37,38</sup>

### Animals and brain slice preparation

The electrophysiological experiments were carried out essentially as described elsewhere.<sup>21,65</sup> Perforated patch clamp recordings were performed from genetically marked (dtTomato) MCH neurons in brain slices of 10–22 weeks old *MCH-Cre; Isl-tdTomato* female and male mice. Animals were kept under standard laboratory conditions, with tap water and chow available *ad libitum*, on a 12 h light/dark cycle. The animals were anesthetized with isoflurane (B506; AbbVie) and decapitated. Coronal slices (280 µm) containing the Lateral Hypothalamus (LH) were cut with a vibration microtome (VT1200, Leica Biosystems) under cold (4 °C), carbogenated (95% O<sub>2</sub> and 5% CO<sub>2</sub>), glycerol-based modified artificial cerebrospinal fluid (GaCSF). GaCSF contained (in mM): 244 glycerol, 2.5 KCl, 2 MgCl<sub>2</sub>, 2 CaCl<sub>2</sub>, 1.2 NaH<sub>2</sub>PO<sub>4</sub>, 10 HEPES, 21 NaHCO<sub>3</sub>, and 5 glucose, adjusted to pH 7.2 with NaOH. Afterward, slices were transferred into carbogenated aCSF at 36°C for 30–40 min and kept at room temperature until further usage for electrophysiological recordings. aCSF contained (in mM): 125 NaCl, 2.5 KCl, 2 MgCl<sub>2</sub>, 2 CaCl<sub>2</sub>, 1.2 NaH<sub>2</sub>PO<sub>4</sub>, 21 NaHCO<sub>3</sub>, 10 HEPES, and 5 glucose, adjusted to pH 7.2 with NaOH. Brain slices were continuously superfused during electrophysiological recordings with carbogenated (95% O<sub>2</sub>; 5% CO<sub>2</sub>) aCSF at a flow rate of ~2.5 mL min<sup>-1</sup>. In all recordings, the aCSF contained 10<sup>-4</sup> M picrotoxin (P1675; Sigma-Aldrich), 5 × 10<sup>-5</sup> M DL-AP5 (DL-2-amino-5-phosphonopentanoic acid; BN0086, Biotrend) and 10<sup>-5</sup> M CNQX (6-cyano-7-nitroquinoxaline-2,3-dione; C127, Sigma-Aldrich) to block ionotropic GABAergic and glutamatergic synaptic input.

### Perforated patch clamp recordings

Current clamp recordings were performed at ~30 °C in the perforated patch clamp configuration. Neurons were identified by their anatomical location in the LH and their tdTomato fluorescence. Electrodes with tip resistances between 4 and 7 MΩ were fashioned from borosilicate glass (0.86-mm inner diameter; 1.5-mm outer diameter; GB150-8P, Science Products) with a vertical pipette puller (PP-830, Narishige). All recordings were performed with an EPC10 patch-clamp amplifier (HEKA Elektronik) controlled by the program PatchMaster (version 2x90; HEKA Elektronik) running under Windows. In parallel, data were recorded using a micro1410 data acquisition interface and Spike 2 (version 7.01, both from Cambridge Electronic Design). Current clamp recordings were sampled at 20 kHz and low-pass filtered at 2.9 kHz with a four-pole Bessel filter. The calculated liquid junction potential between intracellular and extracellular solution was compensated. At the beginning of the experiments, the neurons were depolarized above the threshold.

Perforated patch experiments were conducted using protocols modified from previous studies, as summarized elsewhere.<sup>65</sup> Recordings were performed with a pipette solution containing (in mM): 140 K-gluconate, 10 KCl, 10 HEPES, 0.1 EGTA, and 2 MgCl<sub>2</sub>, adjusted to pH 7.2 with KOH. ATP and GTP were omitted from the intracellular solution to prevent uncontrolled permeabilization of the cell membrane. The patch pipette tip was filled with internal solution and backfilled with internal solution, which contained the ionophore amphotericin B (A4888; Sigma) to achieve perforated patch recordings and 1% biocytin (B4261; Sigma-Aldrich) to label the recorded neuron. Amphotericin B was dissolved in DMSO to a concentration of 40 µg µL<sup>-1</sup> (D8418, Sigma). The used DMSO concentration (0.1–0.3%) had no noticeable effect on the investigated neurons. The ionophore was added to the

modified pipette solution shortly before use. The final concentration of amphotericin B was  $\sim$ 160  $\mu\text{g mL}^{-1}$ . Amphotericin solutions were prepared from undissolved weighted samples (stored at 4 °C protected from light) every recording day. During the perforation process, access resistance ( $R_a$ ) was monitored continuously, and experiments started after  $R_a$  values reached a steady state ( $\sim$ 10–20 min) and the action potential amplitude was stable.

Orexin B (O6262, Sigma) was added to the aCSF and bath-applied to the cells at a concentration of 100 nM for 10 min with a perfusion rate of  $\sim$ 2.5  $\text{mL min}^{-1}$ . The orexin B effect was analyzed by comparing the action potential frequencies measured during 5 min intervals recorded before and at the end of the peptide applications. The neuron's firing rate averaged from 30 s intervals was taken as one data point to analyze the orexin B responsiveness. To determine the mean firing rate and standard deviation, 10 data points were averaged. On the single-cell level the significance of the response was tested using a Mann-Whitney-U-Test. Data analysis was performed using Spike2 (version 7.01; Cambridge Electronic Design), Igor Pro (version 6.37 Wavemetrics), and Prism 9 for macOS (v 9.5.1, Graphpad).

### Single-neuron labeling

To label single cells, 1% (w/v) biocytin was added to the pipette solution. After the electrophysiological characterization, the perforated patch recording was converted to the whole-cell configuration to allow biocytin to diffuse into the cell for at least 30 s. The brain slices were fixed in Roti-Histofix (P0873, Carl Roth) for  $\sim$ 12 h at 4 °C and subsequently rinsed in phosphate-buffered saline (PBS, pH 7.2, 3 times for 20 min each time). Brain slices were incubated in a PBS-based blocking solution containing 1% (w/v) Triton X-100 (PBS-1%TX) and 10% (v/v) normal goat serum (LIN-ENG9010, Biozol Diagnostica) for 30 min at room temperature (RT). Afterward, the slices were incubated for  $\sim$ 20 h at RT with a dsRed rabbit polyclonal antibody (1:1000, Cat# 632496, TaKaRa Bio, RRID: AB\_10013483) in a blocking solution. Brain slices were rinsed in PBS (5 times for 10 min each) and incubated with Alexa 633-conjugated streptavidin (1:400, S21375, Molecular Probes) and the Alexa 488-conjugated goat anti-rabbit IgG secondary antibody (1:200, cat# 111-545-144, Jackson Immunoresearch, RRID: AB\_2338052) for 3 h at RT in PBS. Brains were rinsed in PBS (5 times for 10 min each time, RT), dehydrated in an ascending ethanol series, treated with xylene for 5 min to remove lipids, and mounted in Entellan (1.07960, Sigma-Aldrich). Fluorescence images were captured with a confocal microscope (SP-8, Leica). Scaling, contrast, enhancement, and z-projections were performed with Fiji/ImageJ v2.14.0. The final figures were prepared with Affinity Designer (Ver. 1.10.8; Serif Ltd, Nottingham, UK).

### Perfusion for immunohistochemistry and RNA *in situ* hybridization

Mice were deeply anesthetized and transcardially perfused first with PBS followed by 4% (w/v) paraformaldehyde (PFA in PBS, pH 7.4). Brains were post-fixed in 4% PFA in PBS at 4 °C overnight and lowered in 20% (w/v) sucrose in PBS for 24–48 h. Brains were cut at 20  $\mu\text{m}$  with Leica CM3050 S Research Cryostat.

### Immunohistochemistry

Free-floating sections were washed in PBS and incubated in blocking solutions (PBS containing 0.3% Triton, 3% Normal goat serum) for 1 h, and subsequently incubated for 48 h with primary antibody directed against MCH (1:500; no. M8440, Sigma-Aldrich) in blocking solution at 4 °C. Subsequently, sections were washed 3 times (10 min each) with PBS and incubated with secondary antibody diluted in blocking solution (1:500, Alexa Fluor 647, goat anti-rabbit, A-21244, Invitrogen) for 2 h at room temperature. Finally, slices were rinsed in PBS and mounted.

### RNA *in situ* hybridization (RNAscope)

*In situ* hybridization was performed according to the manufacturer's protocol for RNAscope Multiplex Fluorescent Detection kit v2 from Advanced Cell Diagnostics (ACD). The probes for Ox1R (*Hcrtr1*; no. 466631-C2), Ox2R (*Hcrtr2*; no. 581631-C3), and MCH (*Pmch*; no. 478721-C4) were commercially available by ACD. Sections were mounted on SuperFrost Plus Gold slides (ThermoFisher) and baked at 60 °C for 6 h. Afterward, slides were submerged in Target Retrieval (no. 322000) at 95.0 °C–99.0 °C for 8 min, followed by a brief rinse in autoclaved Millipore water and dehydration in 100% ethanol. A hydrophobic barrier was then created around the sections using an ImmEdge hydrophobic barrier pen (no. 310018). All incubation steps were performed at 40 °C using the ACD HybEZ hybridization system (no. 321462). Sections were incubated with Protease plus (no. 322331) for 25 min. The subsequent hybridization, amplification and detection steps were performed according to the manufacturer's instructions (Multiplex Fluorescent Detection kit v2; no. 323110). For fluorescent probe detection, the fluorophores Opal 520 (PerkinElmer, no. FP1487001KT), Opal 570 (PerkinElmer, no. FP1488001KT), and Opal 690 (PerkinElmer, no. FP1497001KT) were applied at dilutions between 1:500 and 1:2,000. Sections were then mounted with DAPI using Vectashield Antifade Mounting Medium (Vector Laboratories, no. H-1200), cover-slipped in ProLong Gold Antifade Mountant (Thermo Fisher, catalog P36931), and stored in the dark at 4 °C until imaged.

### RNA *in situ* hybridization (BaseScope)

For Ox1R exon 4–6 and Ox2R exon 2 mRNA expression, *in situ* hybridization was performed according to the manufacturer's protocol for BaseScope Duplex Detection Kit (ACD, Cat# 323800). All BaseScope reagents were purchased from ACD unless otherwise stated. The probes for *Pmch* (Mm-*Pmch*, 890511-C2, ACD) were commercially available by ACD. The Probes for Ox1R exon 4–6 and

Ox2R exon 2 were designed by ACD. The Ox1R probe contained 3 oligonucleotide pairs targeting region 505–1043 of *hcrt1* transcript and the Ox2R probe contained 2 oligonucleotide pairs targeting region 343–521 of *hcrt2* transcript. On the day of the assay, sections were dried at 60°C for 4 h, submerged in Target Retrieval reagent at 95°C–99°C for 6 min using a steamer, rinsed in mQH<sub>2</sub>O, and dehydrated in 100% EtOH. The following day, sections were incubated with Protease III for 25 min at 40°C. Hybridization of the probes, amplification, and detection steps were performed according to the manufacturer's protocol. Sections were counterstained with Haematoxylin (Vector Laboratories Inc., H-3404), cover-slipped with VectaMount mounting media (Vector Laboratories Inc., H-5000), and stored in the dark at 4°C until imaged.

**Microscopy and image processing**

Microscopic images of immunohistochemistry and RNA *in situ* hybridization were obtained with an Olympus SLIDEVIEW VS200 digital slide scanner at a 10x magnification (NA: 0.40) for fluorescence imaging and 40x (NA: 0.95) for brightfield imaging. Laser intensities were kept constant throughout all related conditions. The acquired images were processed using Fiji software. For the analysis of *in situ* hybridization images, we counted dots of Ox1R and Ox2R expression in MCH soma and then defined positive cells as those with three or more dots in RNAscope and one or more dots in BaseScope.

**QUANTIFICATION AND STATISTICAL ANALYSIS**

Statistical analyses were performed using GraphPad Prism 10 software (Dotmatics). All data are presented as mean ± SEM. Datasets with only two independent groups were analyzed for statistical significance using an unpaired two-tailed Student's t test. Datasets subjected to two independent factors were analyzed using two-way ANOVA followed by Bonferroni post hoc test. Statistical significance was set at P < 0.05.